JOURNAL OF Applied Polymer SCIENCE

The Use of Poly (ε-caprolactone) to Enhance the Mechanical Strength of Porous Si-Substituted Carbonate Apatite

Le Thi. Bang,[1,2] Giichiro Kawachi,[2] Masaharu Nakagawa,[2] Melvin Munar,[2] Kunio Ishikawa,[2] Radzali Othman[1]

[1]School of Materials and Mineral Resources Engineering, Universiti Sains Malaysia, 14300 Nibong Tebal, Penang, Malaysia
[2]Department of Biomaterials, Faculty of Dental Science, Kyushu University, 3-1-1 Maidashi, Higashi-ku, Fukuoka 812-8582, Japan
Correspondence to: R. Othman (E-mail: radzali@eng.usm.my)

ABSTRACT: Poly(ε-caprolactone) (PCL)/silicon-substituted carbonate apatite (Si-CO3Ap) composite derived from the interconnected porous Si-CO3Ap reinforced with molten PCL was prepared. PCL was used to improve the mechanical properties of a porous apatite by a simple polymer infiltration method, in which the molten PCL was deposited through the interconnected channel of porous Si-CO3Ap. The PCL covered and penetrated into the pores of the Si-CO3Ap to form an excellent physical interaction with Si-CO3Ap leading to a significant increase in diametral tensile strength from 0.23 MPa to a maximum of 2.04 MPa. The Si-CO3Ap/PCL composite has a porosity of about 50–60% and an interconnected porous structure, with pore sizes of 50–150 μm which are necessary for bone tissue formation. These results could pave the way for producing a porous, structured biocomposite which could be used for bone replacement. © 2013 Wiley Periodicals, Inc. J. Appl. Polym. Sci. 130: 426–433, 2013

KEYWORDS: composites; mechanical properties; biomedical applications; biomaterials

Received 12 November 2012; accepted 7 February 2013; published online 18 March 2013
DOI: 10.1002/app.39164

INTRODUCTION

Bone tissues are composed of a biological mineral calcium phosphate (CaP) and about 40 wt % of bio-organic polymers,[1,2] which are responsible for superior strength and partial elasticity for biological calcified tissues.[3] In addition, bone-substituted materials with porous structures have a strong bond with the mineral bone and provide a mechanical interlocking caused by the ingrowth of bone tissues into the pores.[4] Thus, a natural strategy to combine polymers and CaPs to fabricate scaffolds that meet the requirements desired for bone applications have been intensively researched. So far, many researches have showed that the ceramic-polymer composite scaffold has an advantage of the strong compressive strength of ceramic and the flexibility of a ductile polymer.[1,5] However, there has been only limited success in improving the mechanical strength as well as the bioactivity of composite scaffolds through different polymer methods. For example, the porous biocomposites have been prepared with various polymers reinforced with 10–40 vol % hydroxyapatite (HA) by various polymeric processing techniques to improve the osteoconductivity and bioactivity.[6] However, the material became fragile as the HA content was increased, which limited the HA content to 40% or 20%.[7] This decreases the osteointegration of the biocomposite. On the other hand, CaP, such as HA, which has a similar composition with the bone tissue was hybridized with a polymer to improve the biocompatibility of the material.[8] However, it was observed that the addition of HA does not increase the strength over that of the monolithic polymer[3] because the combination of a ceramic powder and polymer is not an easy process which leads to a decrease in mechanical strength when high ceramic powder concentrations was used.[9] Coating of polymers, i.e. poly(lactic acid) (PLA), poly(glycolic acid) (PGA), poly(lactic-*co*-glycolic) acid (PLGA) or poly(ε-caprolactone) (PCL), on the CaP phases is an alternative method for fabricating composite scaffolds to improve both mechanical properties and bioactivity.[5,8,10] However, these polymers are always dissolved in organic solvents before being coated onto the porous CaP. This led to concerns about the residual polymer solvent which might be present in the final product, and can be harmful to the cells.[6,11] In addition, the substrates of these materials were not carbonate apatite (CO_3Ap) or silicon-substituted carbonate apatite (Si-CO_3Ap) but HA, tricalcium phosphate (TCP), or a biphasic calcium phosphate (BCP) because the fabrication of HA or TCP/BCP foams requires high temperatures (i.e., 1200°C and above) which could not be applied to CO_3Ap or Si-CO_3Ap. Furthermore, the bony natural apatites differ from HA in that they contain carbonate ions in significant amounts, from about 3–8

wt %, in the apatite structure[12,13] along with several multi-substituted ions (Si^{4+}, Na^{+}, Mg^{2+}, K^{+}, F^{-}, Cl^{-}, etc.).[14,15] Silicon-substituted apatite was reported to promote the bone remodeling processes.[16] Therefore, a synthetic silicon-substituted carbonate apatite appears to be an excellent candidate for bone substituted material.

Biodegradable and bioresorbable polymer scaffolds developed as substrates for cell tissue regeneration found great application and success in the last few years. Biodegradable polymers, such as PLA, PGA, and their copolymers PLGA, PCL are the most widely biodegradable polymers used for the development of porous three-dimensional scaffolds.[1] They are biocompatible and have been approved by the Food and Drug Administration (FDA) for use in medical applications and drug delivery devices.[17] PLGA is known to support osteoblast migration and proliferation.[18] However, PGA, PLA, and PLGA are too weak to be used in load-bearing application since they reduce the effect of stress-shielding.[1] In addition, their degradation products are relatively acidic causing a strong inflammatory response.[11] On the other hand, PCL has a high toughness, and a high decomposition temperature.[19] PCL showed the sufficient mechanical properties to serve the implant that need to be maintained for at least 6 months.[17] PCL degrades at a significant lower rate than PLA, PGA, and PLGA. This characteristic makes PCL more attractive for long-term implantation.

In this research work, the fabrication of a biocomposite derived from the interconnected porous silicon-substituted carbonate apatite reinforced with molten PCL was developed to mimic the composition and structure of bone coupled with enhanced mechanical performance. The porous PCL/Si-CO_3Ap biocomposites might provide excellent possibilities for the fabrication of artificial bone replacement.

MATERIALS AND METHOD

Preparation of Silicon-Substituted Carbonate Apatite Powder (Si-CO_3Ap)

A precipitation method was adopted to prepare Si-CO_3Ap using $Ca(OH)_2$ (96% purity, Fluka, St. Louis, MO), H_3PO_4 (15M, Merck, Germany), and silicon tetra-acetate [$Si(COOCH_3)_4$] (98% purity, Sigma, St. Louis, MO) with CO_2 gas as the carbonate source. Based on previous research work, in order to obtain a high B-type CO_3Ap with respect to the A-type, the CO_2 flow was set at 0.5 bubble/s as the outlet flux.[20]

According to the chemical formula [eq. (1)] proposed by Gibson et al.[21] for silicon-substituted HA (Si-HA), the amount of reagents were calculated by assuming that one SiO_4 ion would substitute for one PO_4 ion based on a stoichiometric HA, Ca/f(P+Si) molar ratio = 1.67.

$$Ca_{10}(PO_4)_{6-x}(SiO_4)_x(OH)_{2-x} \quad (1)$$

In this research work, the Si content was chosen to be 1.6 wt % which had been shown to be the best amount for the enhancement of the mechanical properties of Si-HA reported in our previous study,[22] where the Ca/P ratio = 1.84. For comparison purposes, the structural characteristics (crystallite size, lattice parameters, and FTIR analysis) of the as-synthesized Si-HA (Si (wt %) = 1.6)[22] were used in this research work.

Preparation of Interconnected Porous Si-CO_3Ap

In this study, wax spheres (200 and 400 μm, YETI Dentalprodukte GmbH, Engen, Germany) were used as a fugitive phase. The wax spheres were mixed with Si-CO_3Ap powders with different wax contents of 40, 60, and 80 wt %. The mixture was homogenized for 12 h using a rolling machine. It was then compacted by an uniaxial hydraulic pressing equipment using a die with 8 mm diameter at a pressure of 10 MPa. The specimen's size is φ 8 mm × 4 mm thickness.

In order to produce porous materials without the decomposition of Si-CO_3Ap, the green body mixtures were heat-treated at 550°C for 7 h (heating rate of 2°C/min) to burn out the wax spheres, followed by sintering at 700°C for 4 h (heating rate of 3°C/min) in CO_2 atmosphere. This heat-treatment regime was to obtain a thermal decomposition of wax sphere without affecting the integrity of the green body. During this burn-out operation, oxygen gas (40 mL/min) was flowed in during the heat-treatment process to promote the oxidation of the organic matter.[23]

Preparation of Porous Si-CO_3Ap/PCL Biocomposite

Porous Si-CO_3Ap/PCL biocomposite (hereafter referred to as biocomposite) was prepared by a vacuum infiltration method. Si-CO_3Ap block was placed in a shrinkable tube, which was connected to an oil vacuum pump. PCL (M_n = 10,000, Wako, Japan) was first melted in a vacuum oven at 90°C and quickly poured onto the surface of Si-CO_3Ap under vacuum to allow the rapid displacement of air by polymer into the porous structure. After 5 min infiltration, the samples were quickly placed in boiling water for 1 min, and further wiped with cotton buds to remove excess polymer at the surface of Si-CO_3Ap blocks. The samples were then dried in an oven at 37°C for 24 h before being characterized.

Characterization

The Si-CO_3Ap powders and compacts were characterized by X-ray diffraction (XRD, D8 Advance A25 Bruker) for phase identification. The CO_3 content of the powders was analyzed using an elemental analyzer (CHN test; Perkin Elmer series 2, 2400 CHNS/O). X-ray fluorescence spectrometer (XRF; Rigaku RIX-300 wavelength dispersive) was used to study the Ca/P ratio of the as-synthesized powders. The lattice parameters (*a* and *c*) of Si-CO_3Ap and Si-HA samples were calculated at the (002) and (300) Miller planes from the XRD patterns. Fourier transform infrared (FTIR; Perkin–Elmer FTIR 2000, FTIR spectrometer) spectroscopy was used to study the Si and CO_3 substitutions of the different functional groups, such as OH^{-}, PO_4^{3-}, CO_3^{2-}, and SiO_4^{4-} in the Si-CO_3Ap sample.

The apparent porosity of the porous Si-CO_3Ap and Si-CO_3Ap/PCL biocomposite compacts were calculated from the dry weight and volume of each specimen. The true density and closed porosity were calculated according to eq. (2) and eq. (3), respectively.[24]

$$\text{True density } (\rho_r) = \left(\frac{m_{\text{dry}}}{m_{\text{dry}} - m_{\text{sub}}}\right) \times \rho_{H_2O} \quad (2)$$

$$\text{Closed porosity } (\%) = \left(1 - \frac{\rho_r}{\rho_{\text{HA}}}\right) \times 100 \quad (3)$$

where m_{dry} is the dry weight in air, m_{sub} is the weight when submerged in deionized water, ρ_{HA} is the theoretical density of HA (assumed to be 3.156 g/cm^3) and ρ_{H_2O} is the density of water at room temperature.

The PCL content of the biocomposite in mass percentage was determined by taking the difference of the masses of the biocomposite and porous Si-CO_3Ap and normalizing the result as a weight percentage of the biocomposite mass according to eq. (4).

$$\text{PCL content (wt \%)} = \frac{m_b - m_s}{m_b} \times 100 \quad (4)$$

where m_b and m_s are the masses of the biocomposite and porous Si-CO_3Ap, respectively.

The initial void space (vol %) of the porous Si-CO_3Ap was estimated by subtracting the volume of the porous Si-CO_3Ap sample determined by measuring its dimensions from the theoretical dense volume and normalizing with the porous Si-CO_3Ap volume.

$$\text{Initial void space (vol \%)} = \frac{\pi\left(\frac{d}{2}\right)^2 h - \frac{m_s}{\rho_s}}{\pi\left(\frac{d}{2}\right)^2 h} \times 100 \quad (5)$$

where d, h, m_s, and ρ_s are the diameter (mm), thickness (mm), mass (g), and density (g/cm^3), respectively of the porous Si-CO_3Ap compact.

The estimated void space of the biocomposite was estimated by subtracting the volume of the theoretical volume of the biocomposite (based on measurements of the mass and density of each of the biocomposite constituents) from the volume of the biocomposite and normalizing the result with the biocomposite volume.

$$\text{Estimated void space (vol \%)} = \frac{\left(\frac{m_s}{\rho_s} + \frac{m_p}{\rho_p}\right) - \frac{m_b}{\rho_b}}{\frac{m_b}{\rho_b}} \times 100 \quad (6)$$

where m_p (g) is the mass of PCL in the biocomposite; ρ_p and ρ_b are the density of the PCL and biocomposite (g/cm^3), respectively.

The fracture surface morphology of the porous Si-CO_3Ap and biocomposite was observed with a scanning electron microscope (SEM: S-3400N, Hitachi High-Technologies Co., Tokyo, Japan) at 15 kV accelerating voltage after gold coating to evaluate the homogeneity of the bulk morphology and the presence of porosity.

The mechanical strength, in terms of diametral tensile strength (DTS), of the porous Si-CO_3Ap and biocomposite compacts was evaluated at a strain rate of 0.5 mm/min. The size of the specimens for DTS testing was φ 7.76 ($\pm$0.05) $\times$ 3.67 ($\pm$0.06) mm thickness.

The DTS strength was obtained using a universal testing machine (AUTOGRAPH, AGS-J, SHIMADZU, Kyoto, Japan).

In this test, a disk sample was placed between two platens and then vertically compressed until it broke.[25] During loading, the applied force was recorded and the tensile strength (F_t) is calculated using eq. (7):

$$F_t = \frac{2P_{max}}{\pi dh} \quad (7)$$

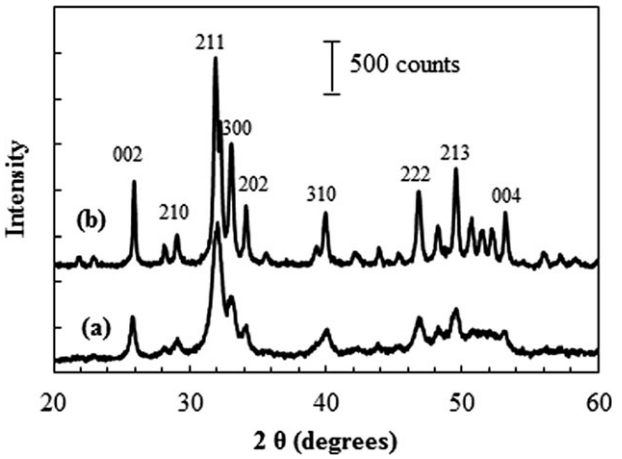

Figure 1. XRD patterns of Si-CO_3Ap powders: (a) as-synthesized Si-CO_3Ap, (b) porous Si-CO_3Ap.

where P_{max} is maximum load at failure (N), h and d are the thickness and diameter, respectively of the compacts (mm).

Statistical Analysis

The results were statistically analyzed by ANOVA with Scheffe's test at a significant level of $P < 0.05$.

RESULTS AND DISCUSSIONS

Physical Properties of the As-Synthesized Si-CO_3Ap and Porous Si-CO_3Ap

Figure 1 shows the XRD patterns of the as-synthesized Si-CO_3Ap and porous Si-CO_3Ap after heat treatment at 700°C. The XRD patterns matched with the ICDD No. 09-432 of HA indicating that pure Si-CO_3Ap was obtained without any secondary phase. In addition, the porous Si-CO_3Ap pattern is narrower and more intense after heat-treatment as a result of an increase in crystallinity. The crystallite size of porous Si-CO_3Ap is smaller than that of the as-synthesized sample, as shown in Table I. The lattice parameters and crystallite size of the as-synthesized Si-CO_3Ap and porous Si-CO_3Ap samples are also listed in Table I. The CO_3 and Si substitutions in HA structure led to changes in the crystal lattice parameters.[15,26] The values presented in Table I are in agreement with previous works,[14,24] in which the *a*-axis decreased and the *c*-axis increased with increasing CO_3 or Si in the HA structure. Incidentally, it was also reported that the *a*-axis decreased in a B-type carbonate apatite.[27] Additionally, the substitution of SiO_4^{4-} and CO_3^{2-} for PO_4^{3-} is assumed to contribute in reducing the crystallite size, as have been observed previously in other studies.[22,26,28]

Table I. Lattice Parameters and Crystallite Size of Si-CO_3Ap Sample

	As-prepared sample			Porous sample
Sample	Crystallite size (nm)	*a* (Å)	*c* (Å)	Crystallite size (nm)
1.6Si-HA[22]	22.81 ± 0.03	9.4505	6.8979	35.61 ± 0.03
Si-CO_3Ap	16.82 ± 0.02	9.4061	6.9057	26.24 ± 0.03

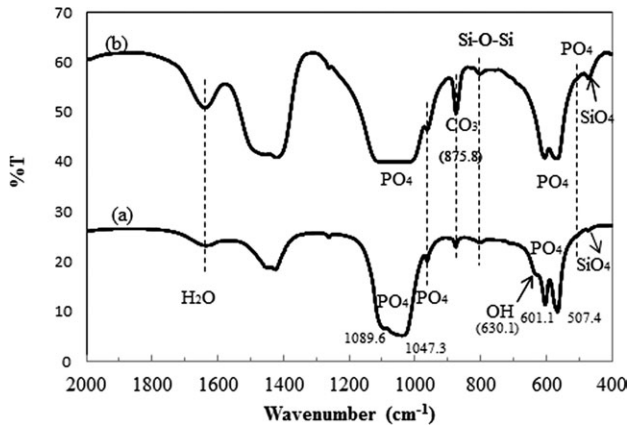

Figure 2. FTIR spectra of as-synthesized powders: (a) silicon-substituted HA,[22] (b) Si-CO_3Ap.

It was hypothesized that SiO_4^{4-} and CO_3^{2-} ions substituting for PO_4^{3-} ions yield a loss of OH^- and Ca^{2+} ions, respectively, to compensate for the different charge of the silicate and carbonate groups.[14,29] The loss of the OH group due to the co-substitution of Si and CO_3 ions for PO_4 ions in the HA structure is confirmed by the FTIR analysis shown in Figure 2. In this Figure, the FTIR spectra of the as-synthesized Si-HA and Si-CO_3Ap samples show similar patterns for all these samples except for the strong CO_3 bands at about 875 cm^{-1} ($\upsilon 2$) in the Si-CO_3Ap sample. The characteristic OH^- band of HA at 630 cm^{-1} is not visible in the FITR spectrum of Si-CO_3Ap sample compared to that of Si-HA sample. In fact, a similar observation regarding the OH signals was also reported due to the substitution of CO_3 at the OH lattice of HA.[30] In this case, the substitution of CO_3^{2-} and SiO_4^{4-} ions for PO_4^{3-} would create an OH^- loss needed to compensate the charge balance.[31,32] In

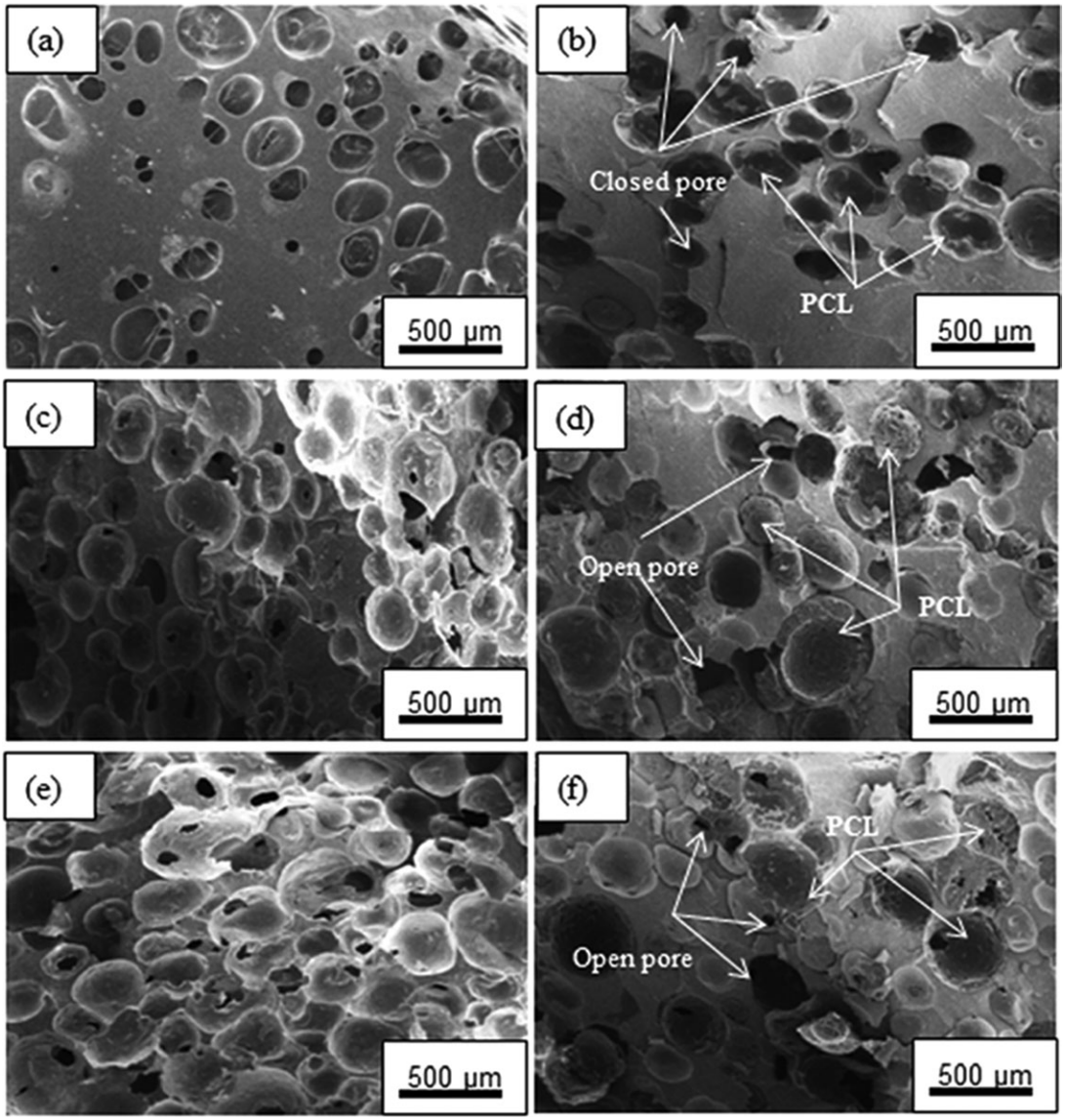

Figure 3. Cross-section SEM images of porous Si-CO_3Ap and Si-CO_3Ap/PCL biocomposite with different wax contents: (a) Si-CO_3Ap-40%, (b) Si-CO_3Ap/PCL-40%, (c) Si-CO_3Ap-60%, (d) Si-CO_3Ap/PCL-60%, (e) Si-CO_3Ap-80%, and (f) Si-CO_3Ap/PCL-80%.

Applied Polymer SCIENCE

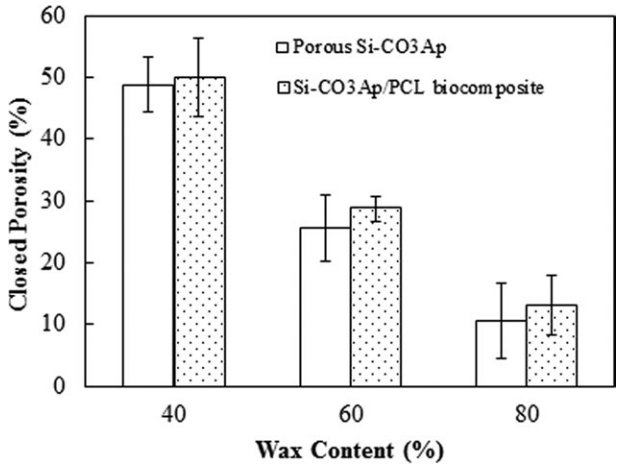

Figure 4. Closed porosity of porous Si-CO_3Ap and Si-CO_3Ap/PCL biocomposite versus the wax contents.

addition, the broad adsorption bands at about 1089 cm^{-1}, 1047 cm^{-1}, 961–962 cm^{-1}, and a shoulder at about 571–601 cm^{-1} corresponding to the PO_4 groups of Si-CO_3Ap are less intense compared to Si-HA sample. This demonstrated that the SiO_4 and CO_3 ions substituted for PO_4 ions in the Si-CO_3Ap.

The Ca/P molar ratio of the as-synthesized Si-CO_3Ap was 2.16, which was higher than the starting value indicating the substitution of the SiO_4, CO_3 ions for the PO_4 ions[12,21] had taken place. The carbonate contents of the powders before and after heat-treatment were 10.25 and 10.04 wt %, respectively. Although the carbonate content value is higher than that in bone, which is 4–8 wt %,[12] the high carbonate content in apatite structure improve significantly both cell adhesion and proliferation.[33]

Porous Structure of Si-CO_3Ap and Si-CO_3Ap/PCL Biocomposite

In this study, the porous structure of Si-CO_3Ap was produced using a volatile porogen, namely, wax sphere, which was removed by heating at 550°C for 7 h in an oxygen-flowing atmosphere to promote oxidation, followed by sintering at 700°C for 4 h in O_2 (40 mL/min) and flowing CO_2 (80 mL/min). This low temperature did not affect the phase transformation of Si-CO_3Ap as indicated in Figure 1.

The cross-section SEM micrographs in Figure 3 show the effect of the wax contents on the porous structure before and after the PCL infiltration. The pores are uniformly distributed throughout the cross-section of the specimen. The pore geometry is similar to the geometry of the starting wax powders added. Prior to PCL infiltration, the Si-CO_3Ap compact shows the presence of open and closed pores, of macro and micro sizes [Figure 3(a,c,e)]. Most of the open pores are due to the volatilization of the wax and appear to be interconnected. The distribution of open and closed pores is estimated to be 15.08–66.53% and 48.87–10.62% at 40–80 wt %, respectively. After the infiltration of molten PCL, followed by removing of excess polymer and a drying process, the macropores in the Si-CO_3Ap are either completely filled with PCL or partially filled with PCL at different extents [Figure 3(d,f)]. However, the open macropores Si-CO_3Ap at 40 wt % wax [Figure 3(b)] are completely filled with PCL, whereas no PCL infiltrated into the closed pores which was the result of wax volatilization (due to low wax content) and the original closed pores in the Si-CO_3Ap [Figure 3(b)]. This can be supported by the closed porosity of the specimens shown in Figure 4. Before PCL infiltration, the porous Si-CO_3Ap has a high closed porosity of about 48.87% ± 4.5 at 40% wax. This closed porosity is lower than the apparent porosity (refer to next section, Figure 8), and so, although the majority of the pores in the Si-CO_3Ap at 40% wax is closed pores there were still open pores obtained, and these pores are filled with PCL. On the other hand, the Si-CO_3Ap at 80% wax has a closed porosity as low as 10.62% ± 6.1 whilst the Si-CO_3Ap at 60% wax has a closed porosity of 25.55% ± 5.3. Therefore, the porous structure of Si-CO_3Ap at 60 and 80 wt % wax are considered to be interconnected structure with open pores. The closed porosity of the biocomposite is also plotted in Figure 4, there is a slight increase of closed porosity, however, the closed porosity of the biocomposite at 80 wt % wax is still very low at about 13.07% after PCL infiltration. This demonstrates that an optimized infiltration process of PCL had been achieved, including the infiltration time and method to remove the excess polymer. Preliminary trials in this work had proven that using a shrinkable tube, under vacuum and a short infiltration time, enhanced the effectiveness of PCL infiltration. Consequently, the porous structure of the biocomposite was retained when compared to the dipping of Si-CO_3Ap block in molten PCL solution under vacuum. As observed in the SEM images, the macropores

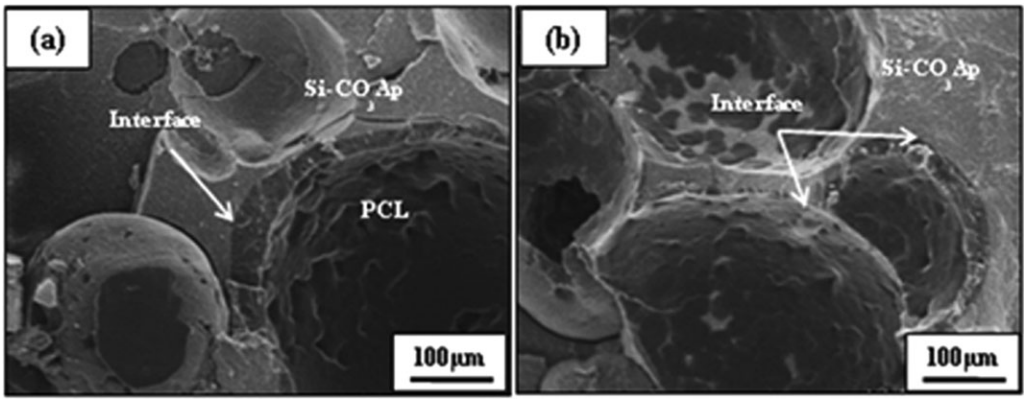

Figure 5. Si-CO_3Ap-PCL interphase: (a) Si-CO_3Ap/PCL-40 wt %, (b) Si-CO_3Ap/PCL-80 wt %.

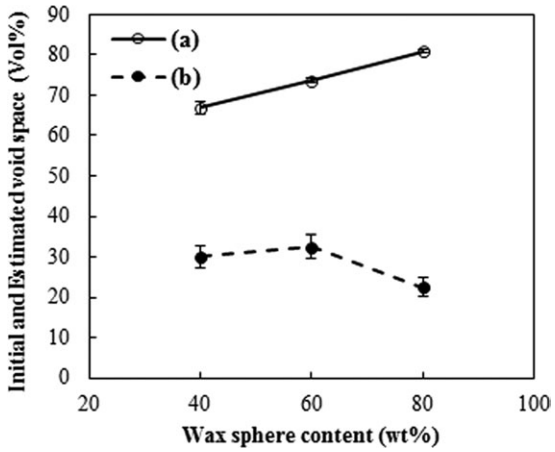

Figure 6. Void space of porous $SiCO_3Ap$ and Si-CO_3Ap/PCL biocomposite versus the wax contents: (a) initial void space, (b) estimated void space.

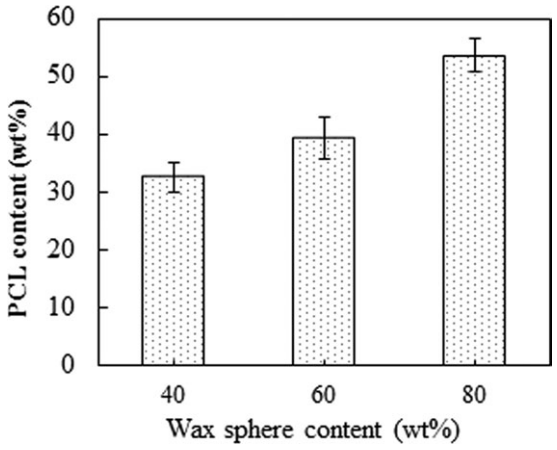

Figure 7. PCL contents of Si-CO_3Ap/PCL biocomposite versus the wax contents.

are not filled completely with the polymer. As a result, the interconnected porosity with a pore size distribution of about 50–150 μm are retained in the final biocomposite at 60 and 80 wt % wax contents.

It was reported that an optimal pore size exists for successful cell infiltration and host tissue ingrowth: 5–15 μm for fibroblasts, 20–125 μm for adult mammalian skin tissues, and 100–350 μm for bone tissues.[5] Additionally, the interconnected pores of 50–200 μm were reported to benefit the circulation of body fluid and the supply of nutrients.[34] Thus, the pore size of 50–150 μm with the interconnected porous structure produced in this study is suitable for the development of artificial bone replacement materials.

Figure 5 shows the Si-CO_3Ap and PCL interface after polymer infiltration. The fracture surfaces showed good adhesion between PCL and Si-CO_3Ap phases. Since no compatibilizers were added, the adhesion is believed to be a physical bonding rather than a chemical bonding. The PCL is well-embedded on the inner walls of the pores of the porous Si-CO_3Ap. This intimate adhesion of PCL to the porous Si-CO_3Ap improves the mechanical strength of the porous Si-CO_3Ap which will be discussed in the next section.

Physical and Mechanical Properties of Porous Si-CO_3Ap and the Si-CO_3Ap/PCL Biocomposite

The initial and estimated void space is shown in Figure 6. The initial void space was the result of macropores after wax removal, as well as the existing porosity in the initial material. The initial void space increases with the increasing wax content. As shown in Figure 6, the initial void space is about 77–80% when using 60 and 80 wt % wax. The high initial void space in combination with the interconnected structure would provide the pathway for PCL infiltration. The retained void space was a consequence of incomplete filling of PCL in order to obtain the porous structure of the biocomposite. The retained void space increased when the wax content increased from 60 and 80 wt % due to the increase of macropores. However, at 80 wt % wax, the retained void space was lower than those of the samples with 40 wt % and 60 wt % wax. This can be explained by the presence of interconnected channels with larger pore size which provide the route for the PCL infiltration through the porous Si-CO_3Ap.

The presence of PCL in the biocomposite is summarized in Figure 7. The PCL content increases with an increase in wax content. This is in agreement with the initial void space (Figure 6). The higher initial void space with interconnected pore allowed the higher PCL content infiltration.

Figure 8(a,b) presents the apparent porosity and DTS, respectively, of the porous Si-CO_3Ap and Si-CO_3Ap/PCL biocomposite. High porosity can be obtained by using high wax contents. The porosity of the porous Si-CO_3Ap is about 64–70%. After PCL infiltration, the porosity of the biocomposite decreases to 50–60%. The decrease in porosity was the result of the PCL infiltration which was evidenced by the SEM images (Figure 3). The infiltration of PCL in the porous Si-CO_3Ap also caused an increase of DTS values as shown in Figure 8(b). It is clearly seen that the DTS of porous Si-CO_3Ap is found to decrease with increasing wax content due to the increase of porosity. However, after PCL infiltration, the DTS of the biocomposite is significantly higher than that of porous Si-CO_3Ap. Additionally, the biocomposites also seemed to be tougher upon PCL infiltration based on observations of the fracture modes during the experiment. The DTS increases approximately seven times for the Si-CO_3Ap/PCL-80 wt % wax and two times for Si-CO_3Ap/PCL-40 wt % wax. This is due to the interconnected porous structure which permitted the infiltration of molten PCL and the excellent adhesion between PCL and Si-CO_3Ap (Figure 5). The DTS value of porous Si-CO_3Ap is about 0.23 (80 wt % Wax)−1.19 (40 wt % Wax) MPa whilst that of the biocomposites have significantly increased to 1.70 (80 wt % wax)–2.04 (40 wt % wax) MPa.

It is apparent that, the introduction of PCL into the porous Si-CO_3Ap has remarkably enhanced the mechanical strength of the interconnected porous Si-CO_3Ap, particularly when the wax content is 80 wt %. The mechanism for improving the strength of the sample can be clearly illustrated by a cross-section at Si-CO_3Ap/PCL interface (Figure 5), where the PCL covered the

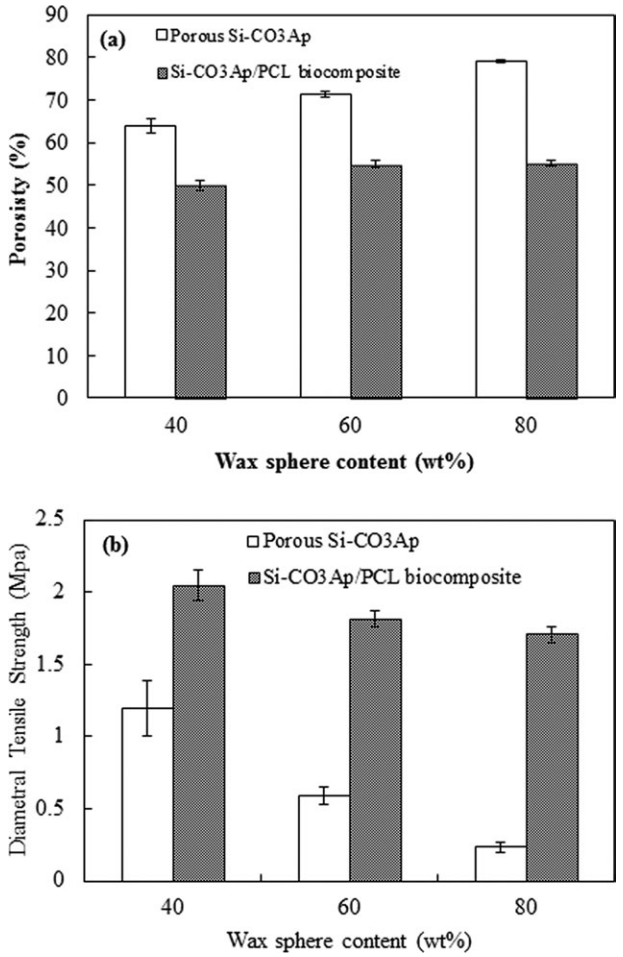

Figure 8. Porosity and DTS values of the porous Si-CO_3Ap and Si-CO_3Ap/PCL biocomposite: (a) Porosity, (b) DTS value.

macropore of the Si-CO_3Ap to form a smooth surface and provide an interpenetrating of ceramic/polymer composite,[5] and so, improved the mechanical strength of the materials. In addition, the uniform distribution of pores might also improve the mechanical properties of the samples.[35]

An attempt was also made to compare the solubilities of PCL and CO_3Ap. However, the values reported were based on tests which could not be compared directly, for instance the solubility of PCL was reported in various solvents,[36] whilst the solubility of CO_3Ap in various buffer solutions had also been studied.[37] Apart from the differences in the use of solvents or solutions, the solubility parameters were also different. It would be an interesting topic to be explored in future works.

CONCLUSIONS

The introduction of the PCL into the porous Si-CO_3Ap structure formed an excellent bonding between the polymer and ceramic phases, resulting in a remarkable improvement of DTS of the final materials from 0.23 to 1.19 MPa to 1.70–2.04 MPa. With increasing PCL content, the DTS value increases dramatically whilst the porosity decreases slowly. The Si-CO_3Ap/PCL biocomposite with 80 wt % wax which possesses a good mechanical strength in combination with a high porosity and adequate pore size is suitable for non-load bearing bone-substitute applications.

ACKNOWLEDGMENTS

This research was financially supported by the AUN/SEED-Net project under the Japan International Cooperation Agency (JICA), MTDC, and the Ministry of Higher Education Malaysia grants.

REFERENCES

1. Dorozhkin, S. J. *Mater. Sci.* **2009**, *44*, 2343.
2. Sun, F.; Zhou, H.; Lee, J. *Acta Biomater.* **2011**, *7*, 3813.
3. Wagoner-Johnson, A. J.; Herschler, B. A. *Acta Biomater.* **2011**, *7*, 16.
4. Sopyan, I.; Mel, M.; Ramesh, S.; Khalid, K.A. *Sci. Technol. Adv. Mater.* **2007**, *8*, 116.
5. Kang, Y.; Scully, A.; Young, D. A.; Kim, S.; Tsao, H.; Sen, M.; Yang, Y. *Eur. Polym. J.* **2011**, *47*, 1569.
6. Converse, G. L.; Conrad, T. L.; Merrill, C. H.; Roeder, R. K. *Acta Biomater.* **2010**, *6*, 856.
7. Tan, K. H.; Chua, C. K.; Leong, K. F.; Cheah, C. M.; Cheang, P.; Abu Bakar, M. S.; Cha, S. W. *Biomaterials* **2003**, *24*, 3115.
8. Roohani-Esfahani, S.-I.; Nouri-Khorasani, S.; Lu, Z.; Appleyard, R.; Zreiqat, H. *Biomaterials* **2010**, *31*, 5498.
9. Supova, M. *J. Mater. Sci. Mater. Med.* **2009**, *20*, 1201.
10. Miao, X.; Tan, D. M.; Li, J.; Xiao, Y.; Crawford, R. *Acta Biomater.* **2008**, *4*, 638.
11. Rezwan, K.; Chen, Q. Z.; Blaker, J. J.; Boccaccini, A. R. *Biomaterials* **2006**, *27*, 3413.
12. Lafon, J. P.; Champion, E.; Bernache-Assollant, D. *J. Eur. Ceram. Soc.* **2008**, *28*, 139.
13. Barralet, J.; Best, S.; Bonfield, W. *J. Biomed. Mater. Res.* **1998**, *41*, 79.
14. Gomes, S.; Nedelec, J.-M.; Jallot, E.; Sheptyakov, D.; Renaudin, G. *Cryst. Growth Design* **2011**, *11*, 4017.
15. Kolmas, J.; Jaklewicz, A.; Zima, A.; Bućko, M.; Paszkiewicz, Z.; Lis, J.; Slosarczyk, A.; Kolodziejski, W. *J. Mol. Struct.* **2011**, *987*, 40.
16. Porter, A. E.; Patel, N.; Skepper, J. N.; Best, S. M.; Bonfield, W. *Biomaterials* **2004**, *25*, 3303.
17. Armentano, I.; Dottori, M.; Fortunati, E.; Mattioli, S.; Kenny, J. M. *Polym. Degrad. Stab.* **2010**, *95*, 2126.
18. Kim, S.-S.; Sun Park, M.; Jeon, O.; Yong Choi, C.; Kim, B.-S. *Biomaterials* **2006**, *27*, 1399.
19. Shor, L.; Güçeri, S.; Wen, X.; Gandhi, M.; Sun, W. *Biomaterials* **2007**, *28*, 5291.
20. Landi, E.; Tampieri, A.; Celotti, G.; Vichi, L.; Sandri, M. *Biomaterials* **2004**, *25*, 1763.
21. Gibson, I. R.; Best, S. M.; Bonfield, W. *J. Biomed. Mater. Res.* **1999**, *44*, 422.
22. Bang, L. T.; Ishikawa, K.; Othman, R. *Ceram. Int.* **2011**, *37*, 3637.
23. Lemos, A. F.; Ferreira, J. M. F. *Mater. Sci. Eng. C* **2000**, *11*, 35.

24. Frank-Kamenetskaya, O.; Kol'tsov, A.; Kuz'mina, M.; Zorina, M.; Poritskaya, L. *J. Mol. Struct.* **2011**, *992*, 9.
25. Kamst, G. F.; Vasseur, J.; Bonazzi, C.; Bimbenet, J. J. *J. Food Eng.* **1999**, *40*, 227.
26. Mostafa, N. Y.; Hassan, H. M.; Abd Elkader, O. H. *J. Am. Ceram. Soc.* **2011**, *94*, 1584.
27. LeGeros, R. Z. *Nature* **1965**, *206*, 403.
28. Boanini, E.; Gazzano, M.; Bigi, A. *Acta Biomater.* **2010**, *6*, 1882.
29. Palard, M.; Champion, E.; Foucaud, S. *J. Solid State Chem.* **2008**, *181*, 1950.
30. Kannan, S.; Vieira, S. I.; Olhero, S. M.; Torres, P. M. C.; Pina, S.; da Cruz e Silva, O. A. B.; Ferreira, J. M. F. *Acta Biomater.* **2011**, *7*, 1835.
31. Landi, E.; Tampieri, A.; Mattioli-Belmonte, M.; Celotti, G.; Sandri, M.; Gigante, A.; Fava, P.; Biagini, G. *J. Eur. Ceram. Soc.* **2006**, *26*, 2593.
32. Pietak, A. M.; Reid, J. W.; Stott, M. J.; Sayer, M. *Biomaterials* **2007**, *28*, 4023.
33. Pieters, I. Y.; Van den Vreken, N. M. F.; Declercq, H. A.; Cornelissen, M. J.; Verbeeck, R. M. H. *Acta Biomater.* **2010**, *6*, 1561.
34. Botelho, C. M.; Brooks, R. A.; Best, S. M.; Lopes, M. A.; Santos, J. D.; Rushton, N.; et al. *J. Biomed. Mater. Res. Part A* **2006**, *79*, 723.
35. Zhao, J.; Duan, K.; Zhang, J. W.; Guo, L. Y.; Weng, J. *Mater. Sci. Eng.: C* **2011**, *31*, 697.
36. Bordes, C.; Freville, V.; Ruffin, E.; Marote, P.; Gauvrit, J. Y.; Briancon, S.; Lanteri, P. *Int. J. Pharm.* **2010**, *383*, 236.
37. Shellis, R. P.; Lee, A. R.; Wilson, R. M. *J. Colloid Interface Sci.* **1999**, *218*, 351.